ISBN: 978-3-95450-227-1 ISSN: 2673-5490 doi:10.18429/JACoW-IPAC2022-WEOYSP1

EXPERIMENTS WITH UNDULATOR RADIATION, EMITTED BY A SINGLE ELECTRON*

I. Lobach†, Argonne National Laboratory, Lemont, IL, USA
S. Nagaitsev[1], A. Romanov, A. Shemyakin, G. Stancari, Fermilab, Batavia, IL, USA
[1]also at The University of Chicago, Chicago, IL, USA

Abstract

We study a single electron, circulating in the Fermilab IOTA storage ring and interacting with an undulator through single and multi-photon emissions. The focus of this research is on single-photon and two-photon undulator emissions. We begin by using one Single Photon Avalanche Diode (SPAD) detector to detect the undulator radiation photons and search for possible deviations from the expected Poissonian photon statistics. Then, we go on to use a two-photon interferometer consisting of two SPAD detectors separated by a beam splitter. This allows to test if there is any correlation in the detected photon pairs. In addition, the photocount arrival times can be used to track the longitudinal motion of a single electron and to compare it with simulations. This allowed us to determine several dynamical parameters of the storage ring such as the rf cavity phase jitter and the dependence of the synchrotron motion period on amplitude.

INTRODUCTION

In our previous experiments [1–3] with an electron bunch we showed that turn-to-turn fluctuations $\mathrm{var}(\mathcal{N})$ of the number of detected undulator radiation photons per turn $\mathcal{N}$ have two contributions: (1) a Poissonian contribution equal to $\langle\mathcal{N}\rangle$, due to the discrete quantum nature of light, and (2) a collective contribution $\propto \langle\mathcal{N}\rangle^2$, related to the interference between the fields generated by the electrons in the bunch. In this paper, we get rid of the collective contribution by considering a single electron circulating in the Integrable Optics Test Accelerator (IOTA) storage ring at Fermilab in order to thoroughly study the quantum fluctuations and verify that they follow the Poissonian photostatistics $\mathrm{var}(\mathcal{N}) = \langle\mathcal{N}\rangle$, predicted by [4–7]. This research is motivated by the surprising observation of sub-Poissonian photostatistics ($\mathrm{var}(\mathcal{N}) < \langle\mathcal{N}\rangle$) in synchrotron radiation reported in Ref. [8] in a similar experiment setting. In addition, we will use the recorded detection times to study the synchrotron motion of a single electron in IOTA [9], similar to previous experiments in Novosibirsk [10, 11].

APPARATUS

In our experiment, a single electron circulated in IOTA with a revolution period of 133 ns and an energy of 96.4 MeV. The undulator parameter is $K_\mathrm{u} = 1.0$ with the number of periods $N_\mathrm{u} = 10.5$ and the period length $\lambda_\mathrm{u} = 5.5$ cm. The wavelength of the fundamental was $\lambda_1 = \lambda_\mathrm{u}(1 + K_\mathrm{u}^2/2)/(2\gamma^2) = 1.16\,\mu$m, where $\gamma = 188.6$ is the Lorentz factor. The second harmonic was in the visible wavelength range. We used a Single Photon Avalanche Diode (SPAD) [12] as a detector, which was mostly sensitive to the visible light with detection efficiency of up to 65 %. We also used two edge-pass filters to only collect the radiation between 550 nm and 800 nm. The radiation was focused on the sensitive area of the detector ($\varnothing 180\,\mu$m) by a single focusing lens with a focal distance of 180 mm, see Figs. 1(a),(b). The radiation was collected in a large angle $> 1/\gamma$. The SPAD detector produced a 10-ns-long TTL pulse at each detection event. Its dead time (20 ns) was shorter than the IOTA revolution period (133 ns). Our data acquisition system (Fig. 1(c)) allowed us to record the revolution number and the arrival time relative to the IOTA revolution marker for each detection event for as long as 1 minute at a time.

PHOTOSTATISTICS MEASUREMENTS

In the optimal focusing, the measured photocount rate was 24.7 kHz, or one photocount per 304 revolutions in IOTA (on average). The dark count rate of the SPAD detector was 108 Hz. In addition, we used a 5-ns-long gate around the expected detection arrival time, which allowed us to reduce the effective dark count rate to 4.0 Hz.

Before any analysis of the photostatistics, it was important to realize that the SPAD detector is binary. It produces the same type of pulses (TTL, 10-ns-long) no matter how many photons are detected per one pass. The collected turn-by-turn data can be represented as a sequence of zeros and ones only. Therefore, we had to alter our original expectation of Poissonian photostatistics to a sequence of Bernoulli trials, i.e., there is a probability p of a detection at every revolution, and a probability $(1 - p)$ of no detection. In our case, $p = (3.29 \pm 0.02) \times 10^{-3}$. Figure 2 illustrates the comparison between the expectation (for a sequence of Bernoulli trials) and the measurement for (a) the distribution of interarrival times and for (b) the distribution of the number of photocounts in a certain time window. In both cases, the χ^2 goodness-of-fit test [13, p. 637] results in a P-value [13, p. 140] above the conventional 0.05 threshold. This means that the null hypothesis (exponential or binomial distribution, respectively) cannot be rejected.

We have also carried out some measurements with an upgraded setup consisting of two SPAD detectors separated by a beam splitter [14]. In this case, the photon number

* The work is supported by the U.S. Department of Energy, Office of Science, Office of Basic Energy Sciences, under Contract No. DE-AC02-06CH11357.
† ilobach@anl.gov

ISBN: 978-3-95450-227-1 ISSN: 2673-5490 doi:10.18429/JACoW-IPAC2022-WEOYSP1

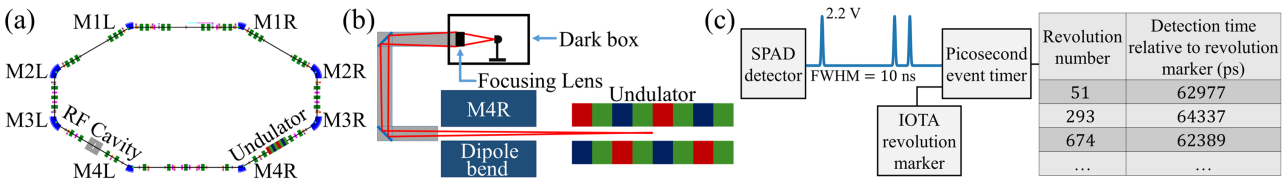

Figure 1: (a) Layout of IOTA, electrons circulate clockwise. (b) Light path from the undulator to the detector (not to scale). (c) Block diagram of the data acquisition system.

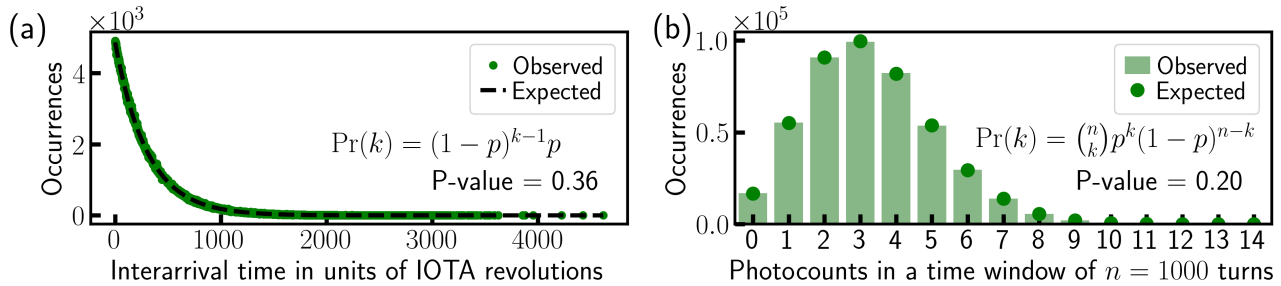

Figure 2: (a) The measured distribution of interarrival times between the photocounts and a fit by a geometric distribution. (b) The measured distribution of the number of photocounts in a time window equal to $n = 1000$ IOTA revolutions and a fit by a binomial distribution.

resolution was improved, since there were three possible outcomes for each pass: 0, 1, or 2 detection events. Still, so far we have not observed anything unusual. There was no statistically significant correlation or anticorrelation in the two detectors.

SYNCHROTRON MOTION STUDIES

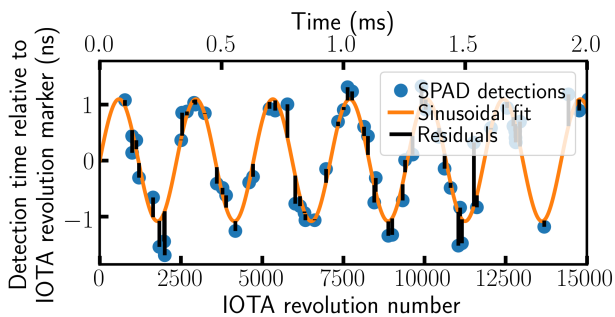

Figure 3: Illustration of the fitting procedure for determination of the synchrotron motion period and amplitude.

Figure 3 illustrates the detection time relative to the IOTA revolution marker as a function of the IOTA revolution number. The observed sinusoidal motion is, in fact, the synchrotron motion of a single electron. The deviations from the sinusoidal fit are due to the time resolution of the SPAD detector (about 0.4 ns rms). On a larger time scale, the amplitude of the synchrotron motion grows and decreases randomly due to the quantum excitation and radiation damping.

We decided to compare the measured arrival times with a simulation of the synchrotron motion. In our simulation [15] we use the following transformation of the relative energy deviation δ_i and the rf phase ϕ_i of a single electron from turn i to turn $i+1$,

$$\delta_{i+1} = \delta_i + \frac{eV_0}{E_0}(\sin\phi_i - \sin\phi_s) - \frac{\langle U\rangle \mathcal{J}_E}{E_0}\delta_i - \frac{U_i - \langle U\rangle}{\beta^2 E_0}, \quad (1)$$

$$\phi_{i+1} = \phi_i - 2\pi q \eta_s \delta_{i+1} + \xi_i, \quad (2)$$

where e is the electron charge, $E_0 = \gamma m_e c^2 = 96.4\,\mathrm{MeV}$, m_e is the electron mass, c is the speed of light, $\beta = \sqrt{1 - 1/\gamma^2}$ is the relativistic velocity parameter, $V_0 = 380\,\mathrm{V}$ is the rf voltage amplitude, $q = 4$ is the rf harmonic number, $\eta_s = \alpha_c - 1/\gamma^2 = 0.070\,83$ is the phase slip factor (variation of η due to variation of γ is negligible), $\alpha_c = 0.070\,86$ is the momentum compaction factor, $\mathcal{J}_E = 2.64$ is the longitudinal damping partition number [16, p. 445], U_i is the radiation energy loss at ith turn, ξ_i is the rf cavity phase jitter at the ith turn. We model ξ_i as a random variable following a normal distribution with a standard deviation σ_ξ. We refer the reader to [16, Eq. (3.28)] for the symplectic part of the transformation. The derivation of the synchrotron damping term, $-\langle U\rangle \mathcal{J}_E \delta_i / E_0$, is described in [16, pp. 438–445]. The quantum excitation term, $-(U_i - \langle U\rangle)/(\beta^2 E_0)$, is considered in [17]. The energy kick at the synchronous phase ϕ_s compensates for the average energy loss due to the synchrotron radiation, i.e., $eV_0 \sin\phi_s = \langle U\rangle$. The average emitted energy per turn in an isomagnetic ring is [16, pp. 434–435] $\langle U\rangle = 8\pi\alpha\gamma u_c/9 = 10.9\,\mathrm{eV}$, where α is the fine-structure constant, $u_c = 3\hbar c\gamma^3/(2\rho) = 2.8\,\mathrm{eV}$ is the critical energy [17, Eq. (11)], $\rho = 70\,\mathrm{cm}$ is the electron trajectory radius in the dipole magnets, $\hbar$ is the reduced Plank constant. The isomagnetic ring approximation works well in IOTA, the radiation in the undulator is negligible compared to the bending magnets. The average number

ISBN: 978-3-95450-227-1 ISSN: 2673-5490 doi:10.18429/JACoW-IPAC2022-WEOYSP1

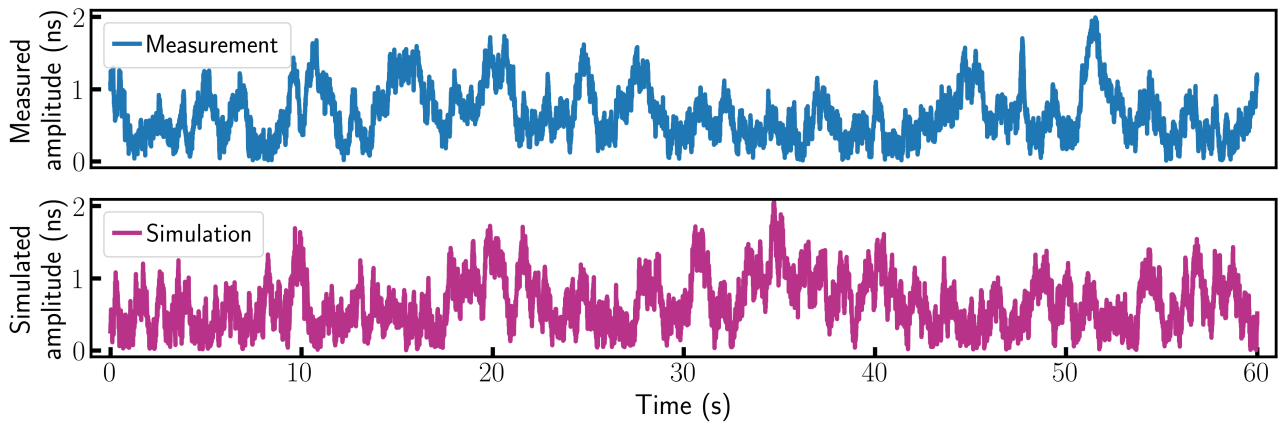

Figure 4: Amplitude of the synchrotron motion of a single electron as a function of time. In the simulation, the rms rf phase jitter is $\sigma_\xi = 6.0 \times 10^{-5}$ rad.

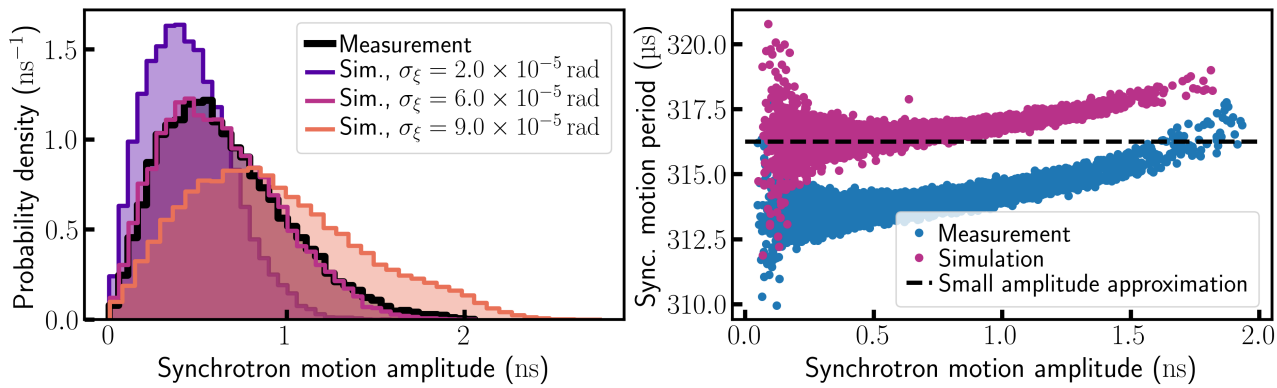

Figure 5: Panel (a) shows the comparison of the measured and simulated distributions of the synchrotron motion amplitude. The best agreement is achieved at the rms rf phase jitter $\sigma_\xi = 6.0 \times 10^{-5}$ rad. Panel (b) shows the synchrotron motion period as a function of the synchrotron motion amplitude.

of photons emitted per turn in an isomagnetic ring is [17] $\langle \mathcal{N} \rangle = 5\pi\alpha\gamma/\sqrt{3} = 12.5$. To simulate the number of emitted photons at ith revolution, we use a Poisson random number generator with the expectation value $\langle \mathcal{N} \rangle = 12.5$. To simulate the energies of these photons, we use the Monte Carlo generator described in Ref. [17]. The sum of these energies gives U_i.

Using our computer code we can generate the data points as in Fig. 3 for a long interval of time, e.g., 1 minute. By fitting the data with short pieces of sinusoidal curves (as in Fig. 3) one can plot the synchrotron motion amplitude as a function of time, see Fig. 4. We cannot compare the measurement and the simulation in this way directly, because it is a stochastic process. However, we can compare the distributions of the synchrotron motion amplitudes. Figure 5(a) illustrates such a comparison, where the simulation results are presented at three different values of the rms rf phase jitter σ_ξ. We can conclude that in IOTA $\sigma_\xi \approx 6.0 \times 10^{-5}$ rad. We considered more values of σ_ξ than illustrated in Fig. 5(a). Further, using the same piecewise sinusoidal fit we can plot the synchrotron motion period as a function of the synchrotron motion amplitude, see Fig. 5(b). Every point in Fig. 5(b) is calculated from a 25-ms-long interval of time. The measured and the simulated synchrotron motion periods agree rather well, which shows that we understand the parameters of the IOTA ring well.

CONCLUSION

To conclude, in our experiment with a single electron and a binary photon detector, we have not yet observed any deviations of the undulator radiation photostatistics from a memoryless Bernoulli process. Our measurements with two SPAD detectors did not reveal any correlation or anticorrelation in the detected photon pairs. Currently, the next phase of experiments is under preparation, namely, the Mach-Zehnder interferometry of undulator radiation [14]. The detection arrival times can be used to study the synchrotron motion of a single electron and to infer some dynamical parameters of the storage ring, such as the rms rf cavity phase jitter and the synchrotron motion period as a function of amplitude. This diagnostics of the longitudinal motion can complement the diagnostics of the transverse motion [18, 19] and facilitate a complete 3D tracking of a single electron in a ring.

ISBN: 978-3-95450-227-1 ISSN: 2673-5490 doi:10.18429/JACoW-IPAC2022-WEOYSP1

REFERENCES

[1] I. Lobach *et al.*, "Transverse beam emittance measurement by undulator radiation power noise," *Phys. Rev. Lett.*, vol. 126, no. 13, p. 134 802, 2021. doi:10.1103/PhysRevLett.126.134802

[2] I. Lobach *et al.*, "Measurements of undulator radiation power noise and comparison with ab initio calculations," *Phys. Rev. Accel. Beams*, vol. 24, no. 4, p. 040 701, 2021. doi:10.1103/PhysRevAccelBeams.24.040701

[3] I. Lobach *et al.*, "Statistical properties of spontaneous synchrotron radiation with arbitrary degree of coherence," *Phys. Rev. Accel. Beams*, vol. 23, no. 9, p. 090 703, 2020. doi:10.1103/PhysRevAccelBeams.23.090703

[4] R. J. Glauber, "Some notes on multiple-boson processes," *Phys. Rev.*, vol. 84, no. 3, p. 395, 1951. doi:10.1103/PhysRev.84.395

[5] R. J. Glauber, "Coherent and incoherent states of the radiation field," *Phys. Rev.*, vol. 131, no. 6, p. 2766, 1963. doi:10.1103/PhysRev.131.2766

[6] R. J. Glauber, "The quantum theory of optical coherence," *Phys. Rev.*, vol. 130, no. 6, p. 2529, 1963. doi:10.1103/PhysRev.130.2529

[7] J.-W. Park, "An investigation of possible non-standard photon statistics in a free-electron laser," Ph.D. dissertation, University of Hawaii at Manoa, 2019. http://hdl.handle.net/10125/66233

[8] T. Chen and J. M. Madey, "Observation of sub-Poisson fluctuations in the intensity of the seventh coherent spontaneous harmonic emitted by a RF linac free-electron laser," *Phys. Rev. Lett.*, vol. 86, no. 26, p. 5906, 2001. doi:10.1103/PhysRevLett.86.5906

[9] I. Lobach, S. Nagaitsev, A. Romanov, and G. Stancari, "Single electron in a storage ring: A probe into the fundamental properties of synchrotron radiation and a powerful diagnostic tool," *Journal of Instrumentation*, vol. 17, no. 02, p. P02014, 2022. doi:10.1088/1748-0221/17/02/p02014

[10] A. Aleshaev *et al.*, "A study of the influence of synchrotron radiation quantum fluctuations on the synchrotron oscillations of a single electron using undulator radiation," *Nuclear Instruments and Methods in Physics Research Section A: Accelerators, Spectrometers, Detectors and Associated Equipment*, vol. 359, no. 1, pp. 80–84, 1995, Proceedings of the 10th National Synchrotron Radiation Conference. doi:10.1016/0168-9002(96)88028-4

[11] I. Pinayev, V. Popik, T. Shaftan, A. Sokolov, N. Vinokurov, and P. Vorobyov, "Experiments with undulator radiation of a single electron," *Nuclear Instruments and Methods in Physics Research Section A: Accelerators, Spectrometers, Detectors and Associated Equipment*, vol. 341, no. 1, pp. 17–20, 1994. doi:10.1016/0168-9002(94)90308-5

[12] *SPCM-AQRH Single-Photon Counting Module*, https://www.excelitas.com/product/spcm-aqrh, Accessed: 2021-5-4.

[13] R. Freund, W. Wilson, and D. Mohr, *Statistical Methods*. Academic Press, Burlington, MA, USA, 2010.

[14] I. Lobach, "Statistical properties of undulator radiation: Classical and quantum effects," Ph.D. dissertation, The University of Chicago, 2021. https://inspirehep.net/literature/1949955

[15] I. Lobach, *The source code for simulation of the longitudinal motion of a single electron in a storage ring* 2020. https://github.com/IharLobach/ursse

[16] S.-Y. Lee, *Accelerator physics*. World Scientific Publishing, 2018.

[17] H. Burkhardt, *Monte Carlo generation of the energy spectrum of synchrotron radiation*, http://cds.cern.ch/record/1038899/files/open-2007-018.pdf, 2007.

[18] A. Romanov, J. Santucci, G. Stancari, A. Valishev, and N. Kuklev, "Experimental 3-dimensional tracking of the dynamics of a single electron in the fermilab integrable optics test accelerator (IOTA)," *Journal of Instrumentation*, vol. 16, no. 12, P12009, 2021. doi:10.1088/1748-0221/16/12/p12009

[19] A. Romanov *et al.*, "3D Tracking of a Single Electron in IOTA," in *Proc. IPAC'21*, Campinas, SP, Brazil, 2021, paper THXB01, pp. 3708–3713. doi:10.18429/JACoW-IPAC2021-THXB01